Significance of glomerular compartmentalization for olfactory coding

Detlev Schild and Helmut Riedel
Physiologisches Institut der Universität Göttingen, Humboldtallee 23, D-3400 Göttingen, Germany

ABSTRACT This paper deals with the dendritic signal processing by mitral cells in the olfactory bulb and its meaning for olfactory coding. The output signals of olfactory receptor neurones are sent to the olfactory bulb where they converge onto the secondary neurones, the mitral cells. On a short time scale, the connectivity between receptor and mitral cells can be assumed to be constant, whereas on a longer time scale, when considering the ongoing de- and regeneration, it is necessary to model the synaptical weights between receptor and mitral cells as variables. In a first approach we used Hebb's rule to this end and presumed that a mitral cell can be represented by one compartment only. In this case, and with a sequence of realistically modeled receptor activity signals, the synaptical weights of all mitral cells converged to the same point though every mitral cell had initial weights different from those of any other mitral cell. This means that a mitral cell, when modeled as one compartment, does not become sensitive to any particular odor quality. A similar lack of quality tuning turned out to occur when one-compartment mitral cells were connected among each other by laterally inhibiting interneurones. We therefore took into account the glomerular fine structure of mitral cell dendrites, assuming electrotonically decoupled dendritic subbranches. This feature together with local inhibitory circuitry at the subbranches led to a fundamentally different type of synaptical convergence pattern. In this case, mitral cells developed differential sensitivities for different odors. Mitral cells have thus to be regarded as multicompartment cells, and local, non-Hebbian learning rules for their afferent synapses are necessary to achieve a reasonable map of odors upon mitral cell activities.

INTRODUCTION

Olfactory receptor neurons (RNs) decode the chemical stimuli of the environment and react to them with complex response profiles (Sicard and Holley, 1984). A typical vertebrate RN responds to many odors with different activities, and the activity profiles vary from cell to cell. This complex structure of RN activities not only allows for a high information capacity, it also leads to the problem that the subsequent system has to evaluate a rather complicated input signal. The receptor signals are conveyed to the olfactory bulb where the axons of receptor cells make synaptical contacts within the glomerula to the secondary neurones (SNs) as well as to interneurons (for a recent review see Halasz, 1990). The functional meaning of the enormous convergence from RCs on SNs is usually seen as: (*a*) a mixture of receptor cell specificities; (*b*) an amplification; and (*c*) an increase in signal to noise ratio (van Drongelen et al., 1978; Schild, 1988).

Especially the first of these points is important here (Freeman, 1974, 1975; Freeman and Schneider, 1982; van Drongelen et al., 1978; Kauer, 1987, 1991; Schild, 1988). The precise impact of this convergence on olfactory coding is not clear, and it is the aim of this paper to further eludicate this point. All models which have dealt with the convergence from RCs to the SNs treat an SN as one compartment (Ahn and Freeman, 1974; Schild, 1986; Li and Hopfield, 1989; Granger et al., 1989). It is well known, however, that mitral cell dendrites ramify considerably within glomerula (Graziadei, 1980, 1986; Halasz, 1990; Pommeroy et al., 1990) so that modeling them by assuming only one compartment per mitral cell does not seem to be appropriate. Considering that the mixing of receptor cell specificities takes place in this highly ramified network, the intraglomerular synapses, their temporal dynamics as well as the manner in which they are modeled, appear to be crucial.

Here we approach the problem of intraglomerular signal processing by simulating a receptor cell activity space according to known discharge properties of olfactory receptor cells. These signals are then taken as input to two different SN models, a one-compartment model and a multicompartment model. The capability of either model of distinguishing between odors is analyzed. It is concluded that modeling an SN as an entity consisting of only one compartment is inappropriate because such secondary model neurons are unable to effectively code different odor qualities whereas multicompartment mitral cells can sample basically the whole input space, i.e., they can become sensitive to virtually every possible odor. Based on glomerular inhibitory mechanisms, they can also perform logical decisions. From these results it

Address correspondence to Dr. Schild.

0006-3495/92/03/704/12 $2.00

appears as if peripheral compartmentalization of SNs together with peripheral inhibition could be a principle of olfactory coding, which is realized in higher vertebrates with typical glomerula but also in lower vertebrates such as goldfish (Ichikawa, 1976) and shark (Dryer and Graziadei, 1991) which rather show a glomerular plexus.

INPUT SPACE OF OLFACTORY RECEPTOR NEURON ACTIVITIES

To model the input to mitral cells as realistically as possible, the main properties of receptor neurone firing characteristics were taken into account (for review, see Getchell, 1986): (*a*) Spontaneous discharges are well below 1 spike/s. (*b*) Maximum firing rates of olfactory neurones when responding to odors are between 5 and 15 spikes/s. (*c*) The statistics of discharges show no apparent regularity; in the case of spontaneous activity they have been approximated as a Poisson process (van Drongelen, 1978) whereas responses to odors are typically of the phasic-tonic type. In the following, only one mean activity is assumed for simplicity so that a response is given just by one value rather than by a time function. (For a more comprehensive model which would take into account also the dynamics of many SNs connected to each other the temporal structure of the input signals would of course be important.) (*d*) Responses show a high degree of reproducibility (Holley et al., 1974). (*e*) Every single (vertebrate) olfactory neuron usually responds to a large number of stimuli though with different activities, and the response profiles of different cells overlap. (*f*) Coding the concentration of one quality over a wide range of concentrations is achieved by more than one neuron. There is very little experimental evidence concerning this point; the concentration range between threshold and saturation of a dose-response curve appears however to be about one logarithmic unit with a variability between half a unit to three logarithmic units (Holley et al., 1974); and (*g*) factor analysis of many responses to many stimuli have revealed that the responses can be described by ~ 10 factors (Revial et al., 1978*a*, 1978*b*, 1982; Sicard, 1986, 1990; Sicard and Holley, 1984).

If there are classes of receptor cells, i.e., ensembles of neurons that respond to an arbitrary sequence of stimuli in the same way, then the number of classes is certainly higher than the number of factors because factor analysis removes correlations between the variables of the original data, i.e., the receptor cell responses (Schild, 1988).

For a model of the olfactory input it does, however, not seem to be crucial to take into account a large number of input classes, it is merely necessary that the numbers of factors and classes are higher than two to exclude a simple topographic one-to-one projection from the first to the second stage of the system. We here assume six independent input variables (it would thus be possible to allow for some correlations between the input classes without necessarily reducing the number of factors below 3).

The program which calculated the responses of receptor cells and their connections to mitral cells was written in "C" and ran on a VME-computer (Motorola MVME 147A-1, UNIX).

Input activities were determined as follows: the six input classes were assumed to respond over eight logarithmic units where the cell's activities were calculated in half-logarithmic steps. For every odor stimulus, we therefore determined 102 values (6 classes times 17 concentrations). For every odor, random variables were drawn from a randon number generator according to the following rules:

(*a*) Choose randomly the number N_a of active classes, $1 \leq N_a \leq 6$.

(*b*) Choose randomly which of the classes are active.

(*c*) Choose for every active class randomly, (*i*) the spontaneous rate r_0, $0 \leq r_0 \leq 0.1(1/s)$, (*ii*) the threshold concentration c_{th}, $0 \leq c_{th} \leq 7.5$, (*iii*) the dynamic range c_d of the dose response curve (in log-units), $0.5 \leq c_d \leq 3$, within which the rate increases from r_0 to saturation r_{max}; and (*iv*) the saturation rate r_{max}, $3 \leq r_{max} \leq 14$, which applies for concentrations $c > c_{th} + c_d$.

(*d*) Repeat the procedures *a–c* for the next stimulus quality.

A set of one hundred qualities was calculated, saved to a file and used as input to the SN models. Fig. 1 illustrates one single input as well as the entire input sample in the state space with the stimulus concentration as parameter. The plot $r_2(r_1)$ describes how r_1 and r_2 increase with stimulus intensity rather than indicating a dependence of r_2 upon r_1. At the lower concentrations, the input vectors are $\vec{r} = (r_1, r_2, \ldots, r_6) \approx (0, 0, 0, 0, 0, 0)$ whereas, for the highest concentration, $\vec{r} = (6.15, 0, 3.4, 9.15, 5.93, 6.96)$.

ONE-COMPARTMENT MODEL OF MITRAL CELLS

We first investigated the behavior of single mitral cells without taking into account inhibitory connections among mitral cells. More precisely, we modeled the peripheral input of mitral cells, i.e., the input they receive through their primary dendrite. So the secondary dendrites, the

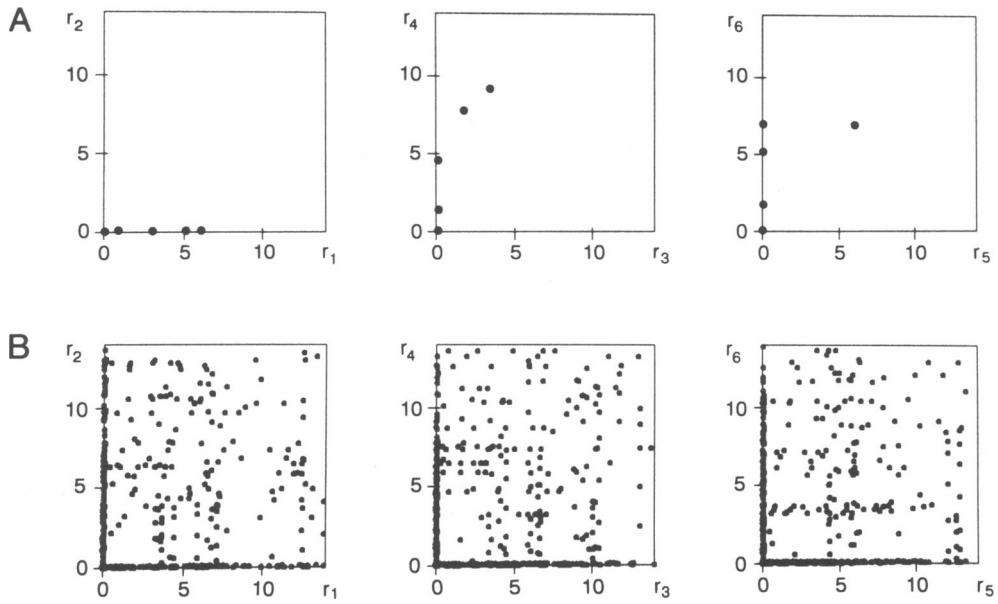

FIGURE 1 (*A*) An example of one simulated stimulus quality over the whole range of concentrations. Five of the six classes are active here, class two is silent. Thresholds and dynamic ranges are different for the different classes, and class 3 and 4 show overlapping dynamic ranges. Class 6 is fully activated before class 5, which has a range of half a logarithmic unit, begins to activate. (*B*) The same sort of presentation for all 100 qualities in all concentrations. The points upon the axes correspond either to inactive classes or to the spontaneous activities of active classes. The remaining points correspond to the randomly chosen activities of active classes. They do not show prevalence in any particular dimension.

soma, as well as the axon, with its collaterals were neglected. For brevity, however, we use the notion mitral cell model or SN model.

One-compartment model of a single mitral cell

A sketch of the model is shown in Fig. 2 A: six inputs r_1 through r_6, i.e., ensemble activities of six receptor cell classes, converge upon one mitral cell the overall input of which is described by the variable m. m can be visualized as the total excitatory generator current of a mitral cell which is eventually responsible for the generation of action potentials in these cells. With c_j being the synaptical strength between input j and this cell, m is simply given by

$$m = \sum_{j=1}^{6} c_j r_j. \tag{1}$$

Because of ongoing degeneration and regeneration of receptor neurons (Breipohl, 1986), the c_j should be considered to be variable. However, very little is known about the dynamics of the c_j. One of the simplest assumptions one can make is that they change according to the correlation of the input r_j and the output m of the synapse:

$$\Delta c_j = \gamma_a m r_j - \gamma_b c_j^3. \tag{2}$$

This is a Hebb rule with nonlinear forgetting (Riedel and Schild, 1991). It has the advantage that the dynamics

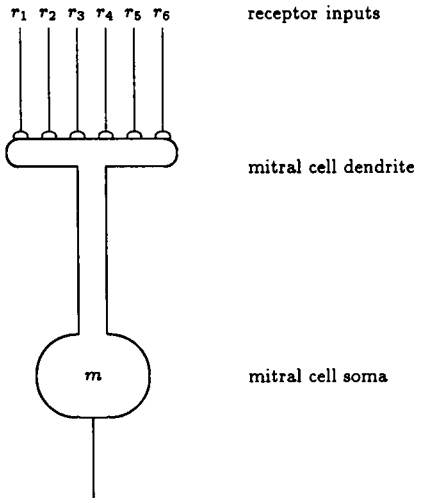

FIGURE 2 One-compartment model of a mitral cell. Six receptor classes r_1 through r_6 converge onto the mitral cell dendrite.

of c_j is intrinsically stable without subsequent normalization of the c_j. γ_a and γ_b are proportionality constants, which can be imagined as the velocities of increase and decrease of the synaptical strength, respectively. The simulation programme ran in the following way: (*a*) Initialize the c_j randomly, (*b*) choose randomly a sequence of input vectors $\vec{r} = (r_1, r_2, r_3, r_4, r_5, r_6)^T$ from the input space as described above, (*c*) calculate the mitral cell variable m according to Eq. 1, (*d*) change the synaptical weights c_j according to Eq. 2 and (*e*) repeat steps *a–d* for the next input vector.

All simulations performed according to this scheme led to stationary values c_j. Fig. 3 shows the six-dimensional space of the synaptical strengths c_j by three two-dimensional projections. The trajectories from eight different initial conditions of the six components of the vector $\vec{c}$ are plotted. The parameters γ_a and γ_b were constant during the iteration so that the trajectories converged to a fixed volume rather than to a fixed point. It is clearly seen that all synaptical strengths have converged to a little fixed volume in the six-dimensional space though the input vectors are randomly distributed in six dimensions. The same held for any other input vector sequence tried. In other words, the pattern $\vec{c} = (c_1, c_2, c_3, c_4, c_5, c_6)^T$ of the c_j does not converge to any particular of the input vectors. Instead it consistently converges to points or vectors which can be shown to be proportional to

$$\vec{e}_1^{(1/3)}: = (e_{11}^{1/3}, e_{12}^{1/3}, e_{13}^{1/3}, e_{14}^{1/3}, e_{15}^{1/3}, e_{16}^{1/3})^T, \qquad (3)$$

with $\vec{e}_1$ being the first eigenvector of the input correlation matrix (Riedel and Schild, 1991). This means that a one-compartment mitral cell does not become particularly sensitive to any of the stimuli except those parallel to the vector $\vec{e}_1^{(1/3)}$.

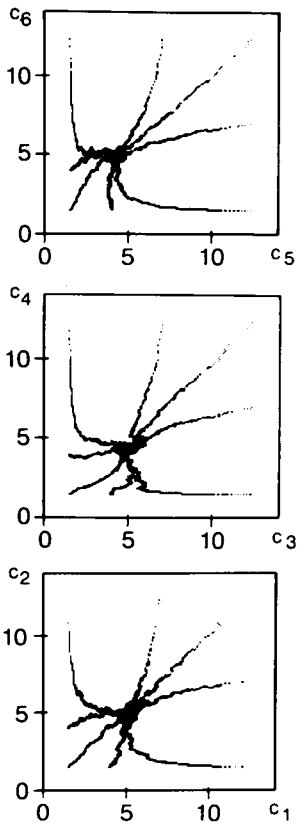

FIGURE 3 Development of the synaptical strengths c_j subjected to the learning rule (Eq. 2). The jagged structure of the trajectories is due to the random input vector sequence. Parameters were $\gamma_a = \gamma_b = 10^{-4}$. The eight initial conditions chosen here lie on a six-dimensional hypercube parallel to the axes of the state space.

Chain of one-compartment mitral cells

It was now intriguing to see whether different mitral cells when connected by lateral inhibition show different convergence patterns, i.e., whether they specialize and become sensitive to some of the input vectors. In this case they would converge to vectors which were not parallel to $\vec{e}_1^{(1/3)}$. Among the many possible geometries of mitral cell connections, we chose a particularly simple one, a closed, one-dimensional chain of mitral cells (indexed by i, see Eq. 4). Inhibition of every cell was assumed to be mediated by the three adjacent cells on either side of every cell. It reduces the variable m_i of the ith mitral cell by a factor which depends on the activities of the six adjacent cells. Modeling inhibition by factors with values between 0 and 1 rather than by a difference takes into account that inhibition in mitral cells occurs predominantly through shunting by opening Cl^--channels (Wellis and Kauer, 1991) rather than by adding negative voltages. The simulation was done in the following steps: (*a*) initialize the connections c_{ij} between input j and mitral cell i randomly, (*b*) choose randomly an input vector $\vec{r}$ from the input space, (*c*) calculate a variable m_i' (before inhibition),

$$m_i' + \sum_{j=1}^{6} c_{ij} r_j \qquad i = 1, 2, \ldots, 14, \qquad (4)$$

(*d*) calculate the variable m_i (after inhibition)

$$m_i = m_i' \prod_{k=-K}^{K} (1 - \mu_k m_{i+k}') \quad i = 1, 2, \ldots, 14; \quad K = 3. \qquad (5)$$

If one of the factors of the product was negative, m_i was set to zero. μ_k represents the inhibitory strength of the kth neighbor of a given cell upon this cell. The rationale for using this equation to calculate inhibition is that the input current m_i' is shortcircuited by a GABA-ergic

mechanism (Mugnaini et al., 1984; Kosaka et al., 1985). (*e*) Change the synaptical weights as before according to

$$\Delta c_{ij} = \gamma_a m_i r_j - \gamma_b c_{ij}^3 \quad (6)$$

(*f*) repeat steps 1 through 5 for the next input.

The result of these simulations was that, as in the case of a single cell, the synaptical weight vectors converged to a straight line. Fig. 4 shows the asymptotic result after 3,030 iteration steps. This line was again parallel to the vector $\vec{e}_1^{(1/3)}$. This asymptotic behavior was shown to be independent from initial values of the connectivities c_{ij} and the strengths of lateral inhibition. Different values for γ_a and γ_b influenced the convergence dynamics as well as the particular asymptotic values c_j. However, the general behavior of the convergence to a straight line was identical. This result means that one-compartment mitral cells do not become sensitive to particular inputs, even if they are connected to each other by lateral inhibitory synapses. Cells with small initial values c_{ij} are simply suppressed by their neighbors and do not influence their neighbors' activities appreciably.

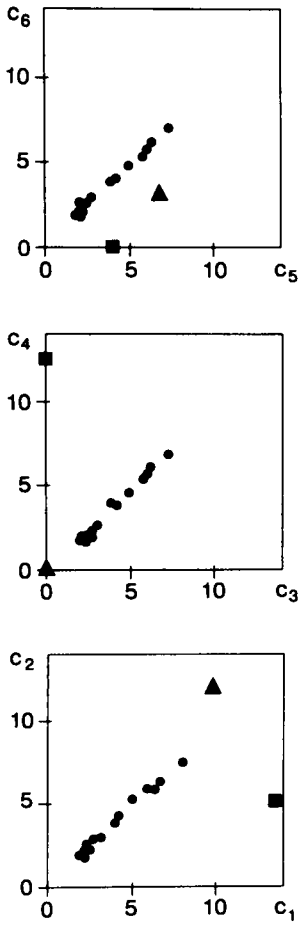

FIGURE 4 Asymptotical distribution of the vectors $\vec{c}_i$ of 14 mitral cells after 3,030 iteration steps. Each point corresponds to the asymptotical solutions of the c_{ij} of one cell. Parameters of the simulation were: $\gamma_a = 4 * 10^{-4}$, $\gamma_b = 10^{-4}$, $K = 3$, $\mu_0 = 0$, $\mu_1 = 0.02$, $\mu_2 = 0.015$, $\mu_3 = 0.01$. Note that γ_a is larger than in the preceding figure. The value $\gamma_a = 10^{-4}$ would lead to smaller c_j because the m_i would be smaller due to the mutual lateral inhibition. The triangles and squares denote two different inputs (stimuli) used in the stimulation shown in Fig. 5.

When the secondary mitral cell dendrites are neglected, the variables m_i would correlate to the mitral cell outputs. In this approximation the m_i would thus indicate mitral cell activities and, for brevity, we will use this term in the following though the m_i actually means the overall input current through the primary dendrite to mitral cell i. It was interesting to compare these activities for different stimuli. Fig. 5 shows the resulting variables m_i for the connectivities given in Fig. 4 and two different stimuli $\vec{r}_A$ and $\vec{r}_B$. The input vectors are represented in Fig. 4 as circles and triangles. Obviously the inputs are fairly different; nonetheless the mitral cells that were activated by $\vec{r}_A$ (Fig. 5, left) were almost the same as those activated by $\vec{r}_B$ (Fig. 5, right), though the activities of the respective cells differ for both stimuli. The same was true for all other stimuli so that some (about half) of the 14 cells coded virtually all stimuli whereas the other cells became relatively silent because they were mostly suppressed and could not gain larger values c_{ij}. Clearly, this is not an efficient way of coding, and it contradicts experimental evidence (Schild, 1987; Scott, 1990).

These results suggested that the assumption of mitral cells that consist of one compartment only might be too restrictive. Instead it appeared as if the morphological fine structure in glomerula had at least roughly to be taken into account by assuming several compartments for different subbranches of the mitral cell dendrite.

MULTICOMPARTMENT MODEL OF SINGLE MITRAL CELLS

In this section we make two assumptions: that the ramifying branches of the primary mitral cell dendrite in a glomerulum are electrotonically independent and that there are local inhibitory interactions from periglomerular cells to mitral cell dendritic branches. Almost nothing is presently known about the electrophysiology of mitral cell dendritic branches. However, with the commonly used value for the specific intracellular resistance (10^6 Ohm μm), a small piece of a dendritic branch of 0.2-μm diameter and 3.14-μm length would have a surface of ~ 2 μm^2 and a longitudinal resistance R_l of 100 M Ohm. The resistance R_t across this membrane piece

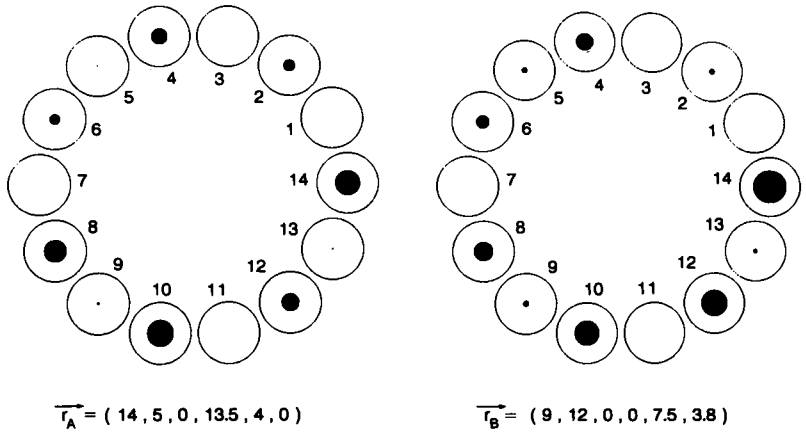

FIGURE 5 Distribution of the activities m_i upon stimulation with two different inputs. Mitral cells are represented in closed chains by open circles and their activities are coded by the radii of the black disks within the circles. The two different stimuli $\vec{r}_A$ and $\vec{r}_B$ used in this stimulation are written below the mitral cell activity patterns; they are also shown in Fig. 4 as squares ($\vec{r}_A$) and triangles ($\vec{r}_B$). Though the input vectors are rather different, the same set of mitral cells are activated.

and the electrotonical length vary with the number of postsynaptic channels open. A density of 50 open channels per μm^2 each having a conductance of ~50 pS would give R_t = 200 M Ohm and an electrotonic length of 4.5 μm. The glomerular diameter is between about 50 and 100 μm, and the dendritic subbranches are presumably many length constants long. Therefore we modeled the mitral cell subbranches as independent. (In a more realistic case some coupling through the potential has to be expected.)

Fig. 6 shows a typical intraglomerular local circuit (Shepherd, 1972): one primary fibre makes contact to a mitral cell microbranch (MCMB) and another primary fiber to a small dendritic process of a periglomerular cell (PGMB), the latter being also connected to the same MCMB. The synapses from primary fibres to the MCMB (c_{ij}) and to the PGMB (d_{ij}) are supposed to be excitatory whereas the synapse from PGMB to MCMB may be reciprocal (f_{ijk}) (Halasz, 1990). Excitatory synapses between periglomerular cells and mitral cells are not taken into account here. The efferent control of periglomerular cells, which might be important in learning, imprinting, and shaping the glomerular specificity, are neither taken into account here because the experimental evidence concerning their function is still controversial. In the following we assume that the synapses f_{ijk} are inhibitory. With such local circuits and all possible combinations of input classes and MCMBs, the network structure of a glomerulum looks as shown in Fig. 7. Though the real biological network is certainly more complex, only the features shown are analyzed here as a first step to investigate intraglomerular signal processing.

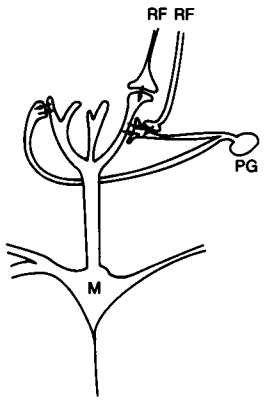

FIGURE 6 Simplified morphological sketch of an intraglomerular circuit. Primary receptor fibres (RF) connect to mitral cell microbranches (MCMBs) as well as to periglomerular cell microbranches (PGMBs). MCMBs and PGMBs are coupled via reciprocal synapses.

Periglomerular cells are also assumed to be compartimentalized due to their intraglomerular, dendritic ramifications. Their microbranches can be stimulated by every input class (synapses d_{ik}). The resulting potentials p_{ik} on the single glomerular branches can then inhibit one, several, or all MCMBs through the synapses f_{ijk}. These effects together with the direct inputs $c_{ij} r_j$ to MCMBs give the potentials m_{ij} on the MCMBs which are finally summed to result in the mitral cell input m_i through the primary dendrite. For simplicity, we chose only two values f_{ijk}, namely f_{ijk} = 0 (no synapse) or f_{ijk} = f = constant (synapses of fixed, constant strength). A

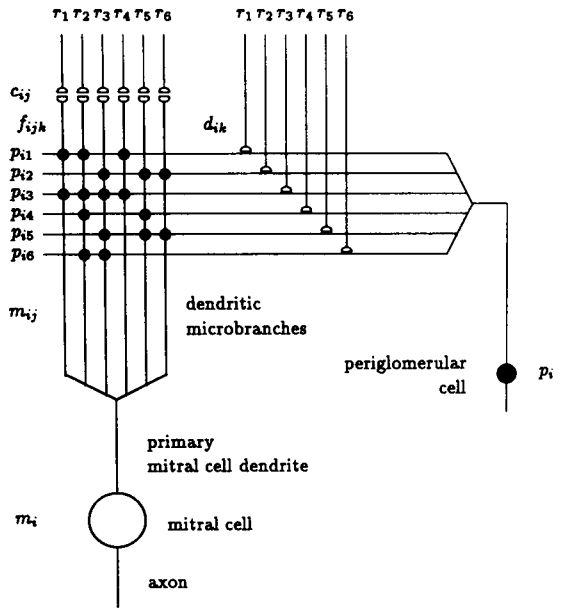

FIGURE 7 Diagram of a simplified intraglomerular circuit. The six receptor classes r_1 through r_6 make contacts to the dendritic microbranches of the mitral cells (synapses c_{ij}) and of the periglomerular cells (synapses d_{ik}). Dendrodendritic synapses (f_{ijk}, *black dots*) between MCMBs and PGMBs are randomly chosen and then held fixed. The MCMBs and PCMBs are indexed by letters j and k, respectively. See text for the definitions of the various quantities.

random variable p in the interval [0, 1] was drawn and f_{ijk} set according to

$$f_{ijk} = \begin{cases} f & \text{for } p < p_s \\ 0 & \text{for } p \geq p_s \end{cases} \quad i = 1, \ldots, 14; \quad j, k = 1, \ldots, 6. \quad (7)$$

For p_s, which is the relative frequency of the dendrodendritic synapses, we chose $p_s = 0.5$, i.e., half of all possible synapses were assumed to exist.

The simulation was done in the following steps: the potentials on the PGMBs were given as

$$p_{ik} = d_{ik} r_k \quad i = 1, \ldots, 14; \quad k = 1, \ldots, 6 \quad (8)$$

whereas the potentials on the MCMBs were

$$m_{ij} = c_{ij} r_j \prod_{k=1}^{6} (1 - f_{ijk} p_{ik}) \quad i = 1, \ldots, 14; \quad j = 1, \ldots, 6. \quad (9)$$

As in Eq. 5, inhibition is modeled by the multiplication with factors between 0 and 1. In the case that one of the factors of the product was negative, m_{ij} was set to zero. m_{ij} corresponds to the input to the jth MCMB of the ith mitral cell. The product reduced this input by a factor depending on all PGMB potentials and the dendrodendritic synapses. Eventually the mitral cell variable m_i is

$$m_i = \sum_{j=1}^{6} m_{ij} = \sum_{j=1}^{6} c_{ij} r_j \prod_{k=1}^{6} (1 - f_{ijk} p_{ik}) \quad i = 1, \ldots, 14 \quad (10)$$

Degeneration and regeneration could affect both the c_{ik} and the d_{ik} synapses. Both were therefore assumed to be subjected to the same type of learning rule, the rule itself being of the same form as in the one-compartment model:

$$\Delta c_{ij} = \gamma_a m_{ij} r_j - \gamma_b c_{ij}^3 \quad i = 1, \ldots, 14; \quad j = 1, \ldots, 6$$
$$\Delta d_{ik} = \delta_a p_{ik} r_k - \delta_b d_{ik}^3 \quad i = 1, \ldots, 14; \quad k = 1, \ldots, 6. \quad (11)$$

However, the meaning of these rules is now fundamentally different from that in the one-compartment model. The changes of synaptical strengths do not depend upon the potentials m_i or p_i but on the local potentials on the microbranches. This means the transition of a Hebbian rule to a local rule which is non-Hebbian and does not imply the correlation of one input with the others.

In all numerical simulations we carried out the synapses c_{ij} and d_{ik} showed a convergence to asymptotically stable values.

A typical asymptotical distribution of the convergence vectors $\vec{c}_i$ is shown in Fig. 8. This simulation was done in parallel for 14 independent mitral cells which were not connected among each other. Initial values were different for all cells. The simulation thus describes the behavior of 14 single cells with differing dendritic structures but without lateral interactions. In this case, a convergence of the $\vec{c}_i$ to the modified eigenvector $\vec{e}_i^{(1/3)}$ was never observed for any randomly chosen initial values. This result did not depend critically upon the parameters. The vectors $\vec{c}_i$ rather showed another conspicuous pattern which can be recognized from the three two-dimensional projections (Fig. 8). Some of the c_{ij} projection points are scattered over the two-dimensional plane, others lie near a line parallel to one of the axes which means that the corresponding vectors have only a low sensitivity to receptor cell inputs that are orthogonal to that line. For instance, the value in the left panel of Fig. 8 marked by a '+' could couple input class 1 to the mitral cell but not (or to a much lesser extent), input class 2. The contrary applies to the value marked by an 'x'. The points near the axes are those which slowly converge to zero, but convergence is extremely slow for small values due to the nonlinear forgetting. The other points in the two-dimensional subspaces, which don't lie on or near a parallel to one of the axes, are responsive to both input classes of the respective subspace. The asymptotical directions of these vectors did never show a

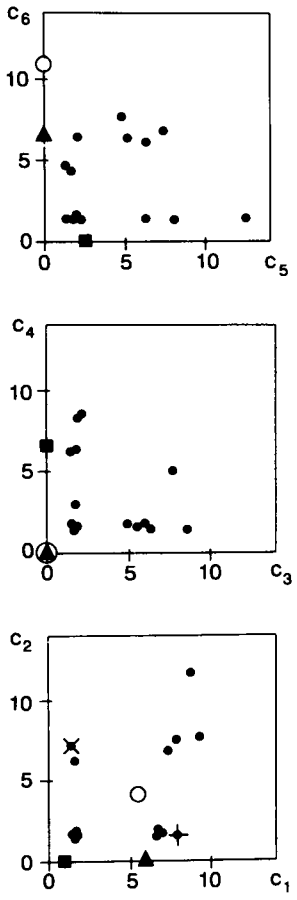

FIGURE 8 Asymptotical distribution of the convergence vectors $\vec{c}_i$ in the multicompartment model. The c_{ij} and d_{ik} were initialized randomly. Parameters were $\gamma_a = 10^{-3}$, $\gamma_b = 10^{-4}$, $\delta_a = 10^{-3}$, $\delta_b = 10^{-4}$, $p_f = 0.5$, $f = 0.01$. The points corresponding to the asymptotical solutions of the c_{ij} are scattered over the planes. The symbols (*squares, triangles, and circles*) indicate three particular inputs used for the simulation shown in the next figure. The interpretation of the c_{ij} marked by a '+' and an '×' are discussed in the text.

convergence to a particular point or line in the input space.

As it is hard to imagine the distribution of the connectivity vectors $\vec{c}_i$ in the six-dimensional space, we give a typical set of asymptotical values c_{ij} in Table 1. In the rightmost column of the Table, the number of values $c_{ij} > 3$ is given for every cell. This number describes for how many input classes the respective cell was particularly sensitive (threshold $c_{ij} = 3$). In the mean, every cell was particularly sensitive to three input classes. The distribution of the d_{ij} was very similar (not shown) because the respective learning rule was identical.

Contrary to the one-compartment model, the multicompartment cell is able to discriminate well between

TABLE 1 **Asymptotical values of the c_{ij} for 14 independent mitral cells**

Cell index i	c_{i1}	c_{i2}	c_{i3}	c_{i4}	c_{i5}	c_{i6}	$c_{ij} > 3$
1	1.78	1.62	**7.72**	**5.00**	1.52	1.42	2
2	**6.71**	1.87	1.94	**8.32**	**12.49**	1.38	3
3	1.56	1.62	**5.46**	1.66	1.62	**4.38**	2
4	**7.87**	1.57	1.64	1.38	**4.72**	**7.73**	3
5	1.34	**7.20**	**8.50**	1.43	1.96	**6.44**	3
6	1.43	1.67	1.45	**6.21**	1.76	1.39	1
7	**9.20**	**7.64**	**5.46**	1.62	2.22	1.34	3
8	**7.80**	**7.53**	1.78	**6.37**	**7.33**	**6.81**	5
9	**7.21**	**6.85**	1.78	**3.01**	**5.16**	**6.44**	5
10	**6.82**	1.76	**4.83**	1.77	**8.02**	1.34	3
11	**6.71**	1.61	1.54	1.77	**6.22**	1.39	2
12	**17.96**	2.30	**6.27**	1.52	1.37	**4.70**	3
13	1.58	**6.23**	**5.97**	1.80	**6.22**	**6.13**	4
14	**8.69**	**11.70**	2.04	**8.45**	1.40	1.49	3

The values were taken after 4,000 iteration steps. Values $c_{ij} > 3$ are printed in bold face.

different input vectors. The Fig. 9 *A*, *B*, and *C* show this ability for three different input vectors. The representation of the 14 independent mitral cell inputs is analogous to Fig. 5. Additionally, the synaptical connectivities f_{ijk} are given as matrices next to every mitral cell. A black circle in a matrix stands for an inhibitory synapse. The matrices have the same meaning and orientation as in Fig. 7: vertical and horizontal lines correspond to MCMBs and PCMBs, respectively. The input vectors $\vec{r}_A$ and $\vec{r}_B$ in the Fig. 9 *A* and *B* are fairly different: they have a large euclidean distance and their mitral cell patterns are very different from each other and can be easily distinguished. On the other hand, input vector $\vec{r}_B$ (Fig. 9 *B*) is similar to input vector $\vec{r}_C$ (Fig. 9 *C*) and so are the corresponding mitral cell patterns (for the problem pattern similarity see Discussion).

Different from the one-compartment model which mapped all input vectors onto similar mitral cell activity patterns, the multicompartment model maps only similar inputs on similar mitral cell activity patterns whereas different inputs result in well distinguishable mitral cell activity patterns. This result was consistent in a large number of simulations with varying parameters and varying initial synaptical weights; exceptions were never observed.

DISCUSSION

It is generally a problem and often impossible to study systems without precise knowledge of their input. This appears to be a problem in understanding olfactory

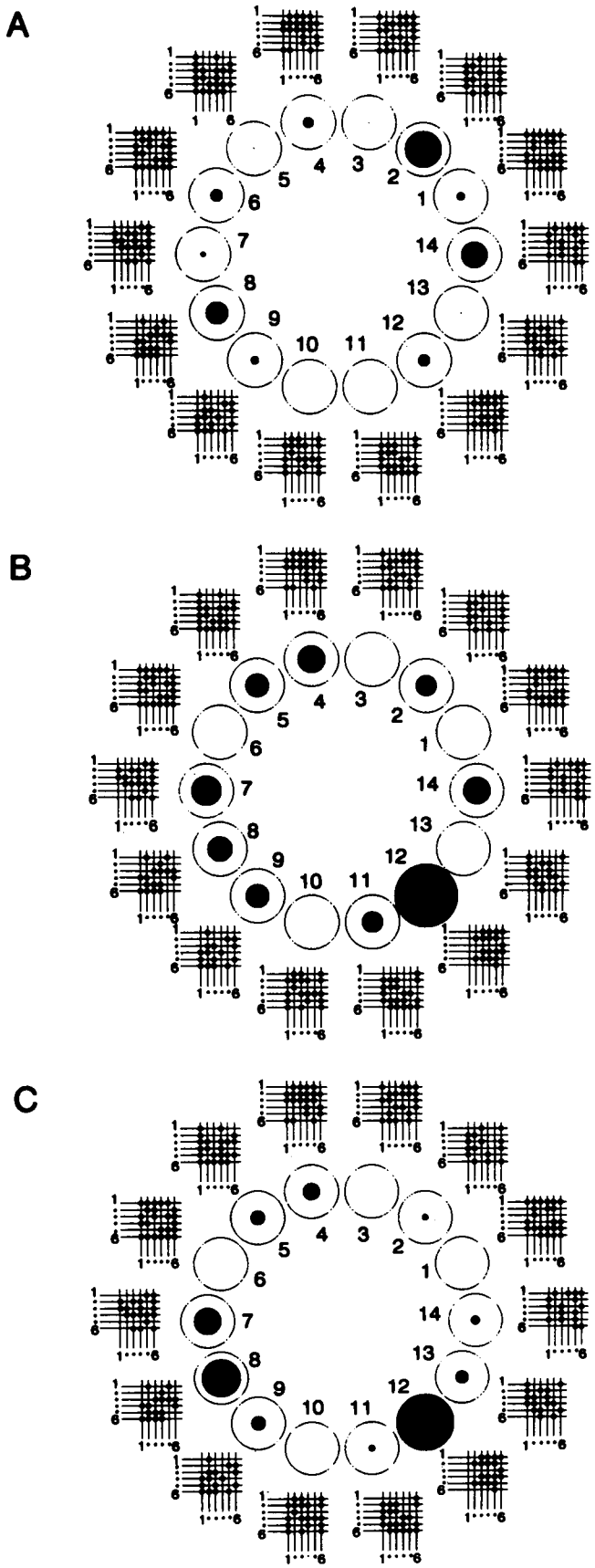

coding and, in particular, signal processing in the olfactory bulb because the interactions of odors with receptor neurons as well as the transduction processes within these cells are not yet fully understood though considerable progress has been made (e.g., Firestein, 1987, 1989, 1990; Kurahashi, 1989, 1990; Schild, 1989; Schild and Bischofberger, 1991; Breer et al., 1990*a*, *b*; Buck and Axel, 1991). In our simulations we tried to circumvent this problem by assuming receptor cell classes and by modeling their activities according to the known response characteristics of olfactory receptor cells. The number of cell classes is not crucial for the model; there might be six as in the special case delineated above or thousands. However, there have to be more than two or three to meet a particular feature of the first olfactory map from receptor cells to glomerula, i.e., the fact that there is no simple topographical map for a two-dimensional surface (the mucosa) to another one (the mitral cell layer). Such a map would be topological in the strict sense, if all points of a certain small area of the former surface would be unambiguously mapped onto a contiguous area of the latter surface. This is certainly not the case in the receptor cell to mitral cell map (e.g., Kauer, 1991).

Relating points and small areas of the mucosa to points and areas of the bulb might even be misleading from a functional point of view. It rather seems more reasonable to consider receptor cell specificities (rather than the geometrical position of receptor cells) as starting "points" of the map. Imagine you could displace receptor cells in the mucosa from their actual positions to arbitrary other positions leaving their axons and connections to the bulb intact; virtually nobody would expect that the bulbar activity image of the odor would be altered by such a change. We therefore assumed that specificities intrinsic to receptor cell classes are mapped on the glomerula.

A number of models of the receptor cell to mitral cell map have been proposed (e.g., Ahn and Freeman, 1974; Schild, 1988; Li and Hopfield, 1989); all of them have in common that mitral cells are regarded as one-compartment entities. Most of these models regard either the

FIGURE 9 Distribution of the activities of the mitral cells upon stimulation with three different input vectors. The synaptical connection pattern f_{ijk} to every mitral cell is shown schematically. A black circle at the crossing of an MCMB and a PGMB stands for an inhibitory synapse, a simple crossing of the dendrites means no synapse. (*A*) Activation of the mitral cells for a particular input vector $\vec{r}_A$ (*squares* in Fig. 8). (*B*) Activation of the mitral cells for a second input vector $\vec{r}_B$ (*triangles* in Fig. 8), which is markedly different from $\vec{r}_A$. The corresponding activity profiles of Fig. 9 *A* and *B* are different, too. (*C*) Activities of the mitral cells for a third vector $\vec{r}_C$ (*open circles* in Fig. 8), which is similar to $\vec{r}_B$. The mitral cell activities in *B* and *C* show similar profiles upon stimulation with $\vec{r}_B$ and $\vec{r}_C$.

spatio-temporal dynamics within the olfactory bulb (Kauer, 1991; Freeman and Skarda, 1985) or cortical signal processing (Granger et al., 1989). The connections between receptor cells and SNs are usually considered fixed in these models. As far as we know, however, the actual dynamics between receptor cells and mitral cells have not yet been modeled at all. To do this, at least in a first approximation, was the primary goal of this paper. The outcome of a one-compartment mitral cell model was disappointing: the synaptical weights c_{ij} between receptor cell classes and mitral cells showed dynamics which led to an asymptotic state in which the c_{ij} are proportional to a root of the first eigenvector of the input correlation matrix. The synaptical weights did not become optimally sensitive to any of the applied stimuli. From a heuristic point of view one might have expected that lateral inhibition between the primary mitral cell dendrites would lead to different orientations of the vectors $\vec{c}_i$ of different mitral cells and thereby to a higher sensitivity of mitral cells to particular stimuli. But the model showed that this was not the case.

The reason for this result is the learning algorithm of the c_{ij}: after the calculation of the scalar product $m'_i = \vec{c}_i \vec{r}$ all information about the direction of the vector $\vec{r}$ in the input space is lost, and the lateral inhibition by granule cells occurs only after this information is lost. In this model the input to the mitral cells can thus not code different orientations of the input space, i.e., different qualities.

As a consequence, different mitral cells can become selective for different stimuli of the input space, only if interactions take place before an integration over the input classes is performed. Though the details of the intraglomerular connectivities are only partially known, there is sufficient morphological evidence for mitral cell dendritic subbranches as well as for the fact that there are inhibitory synapses within glomerula before the small mitral cell dendritic branches enter the primary dendrite (Halasz, 1990).

The above described model incorporates these intraglomerular features (Fig. 7) and is thus more complex than an one-compartment model. The dynamics of synaptical weights c_{ij} in this model led to asymptotically stable states which were "fixed volumes" rather than fixed points due to the continuously varying input. In this multicompartment model different mitral cells were sensitive to different stimulus qualities. The notions 'similar' or 'different' stimuli and 'similar' or 'different' patterns are used here in a qualitative way. An exact treatment is rather complex especially in the context of coding several concentrations of the same odor. It generally appears that there are presently no unique and appropriate measures for the similarities and differences of odors at receptor cell and mitral cell level. We therefore have to exclude this problem here.

The result of differential tuning of mitral cells described here is brought about by the local non-Hebbian dynamics (Eq. 11) together with inhibition at highly differentiated connections within glomerula, i.e., mitral cells with relatively many inhibitory synapses at their jth microbranch are not likely to develop a sensitivity for the jth input class because excitation of this microbranch is often shortcircuited via periglomerular cells by other input classes which are active at the same time. On the other hand, with no or only a few inhibitory synapses on the jth MCMB, there is a high probability for the jth synaptical weight c_{ij} to increase. It is also interesting to note that the multicompartment model is capable of mapping more than merely a weighted superposition of inputs. The activity-dependent inhibition allows quasilogical operations. If there are, e.g., many inhibitory synapses on the kth row of a microbranch of a mitral cell, this corresponds to a logical NAND with respect to this class (k). If input class r_k is active, such a mitral cell would get only a small input, if any. This feature can be illustrated with respect to mitral cell 4 in Fig. 9 *A*, *B*, and *C*. The second row of its glomerular connectivity matrix f_{ijk} consists exclusively of inhibitory synapses. With input vector $\vec{r}_B$ (Fig. 9 *B*), input classes 1 and 6 are active, leading to an about average value m_4 of mitral cell M_4. With input vector $\vec{r}_C$ (Fig. 9 *C*) class 2 is also active. Due to the inhibitory action of class 2 upon mitral cell 4, the mitral cell input m_4 decreases even though the intensity of input vector $\vec{r}_C$ is larger than that of input vector $\vec{r}_B$. This means that the glomerular network is more than a simple linear classifier. Generally, it is able to become sensitive to any region of the input space. Which region this is in any particular case depends on the values of f_{ijk}.

In this context it has been considered that GABAergic periglomerular cells are subject to efferent input from the brain to the bulb, and this obviously could modify the network dynamics through its impact on the periglomerular potentials p_{ik}. We sampled and used a large variety of the mentioned parameters and found that the synaptical weights c_{ij} of a mitral cell can be driven to virtually any wanted orientation of the input space. So one main feature of the multicompartment model became evident: the assumed intraglomerular ramifications and connections are sufficient to map any stimulus quality with high sensitivity and differently from other qualities.

Two related morphological issues need to be discussed here, first, the possible presynaptical inhibition of primary fibres and the possible role of lateral inhibition which follows the glomerular network.

Inhibitory synaptical contacts of periglomerular cells onto primary fibres would, according to Eq. 9, not

change the present model at all; pre- and postsynaptical inhibition have the same effect with respect to the synaptical strengths and their dynamics. One might, however, imagine a slightly extended model in which more than one receptor class converges to one MCMB. In this case, in which Hebbian learning occurs at single MCMBs, the presynaptic inhibition would simply prevent the inhibited receptor cell classes to act on the MCMBs whereas other, noninhibited receptor cell classes could act on these microbranches. On the other hand, postsynaptic inhibition could suppress the action of all inputs to the respective MCMB. Presynaptical inhibition would thus appear to be a more selective inhibitory mechanism.

Lateral inhibition between adjacent mitral cell dendrites has not yet been investigated experimentally in depth. Its role can therefore be imagined easily only in the case of homogenous lateral inhibition between mitral cells. In this approximation, its action would be a contrast enhancement of the images of the mitral cell activities. From a teleological point of view, this or a similar mechanism would seem to be advantageous because the network described here guarantees merely that similar odors are mapped to simlar mitral cell input patterns. However, we can often distinguish well between similar odors, i.e., we do not categorize them as identical, and we therefore need a signal processing step which increases the differences between similar images of similar stimuli. Lateral inhibition mediated by granule cells could serve this purpose.

The model delineated above can also be viewed from a more general perspective: Hebbian learning, in its common form suited for the detection of correlations, does not seem to be appropriate for detecting and discriminating points in a high-dimensional input space such as the space of olfactory neurone activities. To this purpose, mechanisms which include synaptic modifications as well as inhibition in electrotonically partially independent subbranches of dendritic trees, appear to be more potent. Such mechanisms could also be present in other parts of the brain where highdimensional information is processed, e.g., in the network between mossy fibers and granule cells in the cerebellum or in the peripheral dendritic branches of pyramidal cells.

A further interesting point is the different morphology of mitral cells in higher vertebrates and those in some lower vertebrates such as the goldfish. These species show a glomerular plexus rather than typical round-shaped glomerula. If a multicompartment glomerular network as described above is necessary to decode odors, how does odor decoding work in these species which lack typical glomerula? The answer could be the following: in lower teleosts mitral cells have more than one primary dendrite entering the glomerular plexus and there are inhibitory and reciprocal synapses between granule cell dendrites and peripheral mitral cell dendrites (Ichikawa, 1976). What occurs in the periphery of one mitral cell dendrite can be assumed to be at least partly independent from what occurs in another. This means that, also in the case of lower vertebrates, more than one compartment has to be taken into account.

This would indicate that synaptical changes in independent peripheral compartments together with peripheral inhibition could be a common feature of olfactory coding occurring both in species which have glomerula and those which have a glomerular plexus.

Received for publication 24 July 1991 and in final form 28 October 1991.

REFERENCES

Ahn, S. M., and W. J. Freeman. 1974. Steady-state and limit cycle activity of mass of neurons forming simple feedback loops(I): lumped circuit model. *Kybernetik.* 16:87–91.

Breer, H., I. Boekhoff, and E. Tareilus. 1990*a*. Rapid kinetics of second messenger formation in olfactory transduction. *Nature (Lond.).* 345:65–68.

Breer, H., I. Boekhoff, J. Strotmann, K. Raming, and E. Tareilus. 1990*b*. Molecular elements of olfactory signal transduction in insect antennae. *In* Chemosensory Information Processing. D. Schild, editor. Springer, Berlin.

Breipohl, W. 1986. Ontogeny of Olfaction. Principles of Olfactory Maturation in Vertebrates. Springer, Berlin.

Buck, L., and R. Axel. 1991. A noval multigene family may encode odorant receptors: a molecular basis for odor recognition. *Cell.* 65:175–187.

Dryer, L., and P.P.C. Graziadei. 1991. Morphology and cytoarchitecture of the elasmobranch olfactory bulb. *ACHEMS.* 13:252.

Firestein, S., and F. Werblin. 1989. Odor-induced membrane currents in vertebrate-olfactory receptor neurons. *Science (Wash. DC).* 244: 79–82.

Firestein, S., and F. S. Werblin. 1987. Grated currents in isolated olfactory receptor neurons of the larval tiger salamander. *Proc. Natl. Acad. Sci. USA.* 84:6292–6296.

Firestein, S., G. M. Shepherd, and F. S. Werblin. 1990. Time course of the membrane current underlying sensory transduction in salamander olfactory receptor neurons. *J. Physiol. (Lond.).* 430:135–158.

Freeman, W. J. 1974. Topographic organization of primary olfactory nerve in cat and rabbit as shown by evoked potentials. *Electroencephalogr. Clin. Neurophysiol* 36:33–45.

Freeman, W. J. 1975. Mass Action in the Nervous System. Academic Press, New York.

Freeman, W. J., and W. Schneider. 1982. Changes in spatial patterns of rabbit olfactory EEG with conditioning to odors. *Psychophysiology.* 19:44–56.

Freeman, W. J., and C. A. Skarda. 1985. Spatial EEG patterns, non-linear dynamics and perception: the neo-Sherrington view. *Brain Res. Rev.* 10:147–175.

Getchell, T. V. 1986. Functional properties of vertebrate olfactory receptor neurons. *Physiol. Rev.* 66:772–817.

Granger, R., J. Ambros-Ingerson, and G. Lynch. 1959. Derivation of encoding characteristics of layer II cerebral cortex. *J. Cognitive Neuroscience.* 1:61–87.

Graziadei, P. P. C., and G. A. Monti Graziadei. 1980. Neurogenesis and neuron regeneration in the olfactory system of mammals. III. Deafferentation and reinnervation of the olfactory bulb following section of the fila olfactoria in rat. *J. Neurocytol.* 9:145–162.

Graziadei, P. P. C., and G. A. Monti Graziadei. 1986. Principles of organization of the vertebrate olfactory glomerulus: an hypothesis. *Neuroscience* 19:1025–1035.

Halasz, N. 1990. The Vertebrate Olfactory System. Akademiai Kiado, Budapest.

Holley, A., A. Duchamps, M.-.F. Revial, and A. Juge. 1974. Qualitative and quantitative discrimination in the frog olfactory response: analysis from electrophysiological data. *Ann. NY Acad. Sci.* 237:102–114.

Ichikawa, M. 1976. Fine structure of the olfactory bulb in the goldfish, *Carassius auratus. Brain Res.* 115:43–56.

Kauer, J. S. 1987. Coding in the olfactory system. John Wiley and Sons, Inc., New York.

Kauer, J. S. 1991. Contributions of topography and parallel processing to odor coding in the vertebrate olfactory pathway. *Trends Neurosci.* 14:79–85.

Kosaka, T., Y. Hataguchi, K. Hama, I. Nagutsu, and J.-Y. Wu. 1985. Coexistence of immunoreactivities for glutamate decarboxylase and tyrosine hydroxylase in some neurons in the periglomerular region of the rat main olfactory bulb. Possible coexistence of gamma-aminobutyric acid (GABA) and dopamine. *Brain Res.* 343:166–171.

Kurahashi, T. 1989. Activation by odorants of cation-selective conductance in the olfactory receptor cell isolated from the newt. *J. Physiol (Lond.).* 419:177–192.

Kurahashi, T., and T. Shibuya. 1990. Ca^{2+}-dependent adaptive properties in the solitary olfactory receptor cell of the newt. *Brain Res.* 515:261–268.

Li, Z., and J. J. Hopfield. 1989. Modeling the olfactory bulb and its neural oscillatory processings. *Biol. Cybern.* 61:379–392.

Mugnaini, E., F. G. Wouterlood, A. L. Dahl, and W. H. Oertel. 1984. Immunocytochemical identification of gabaergic neurons in the main olfactory bulb of the rat. *Arch. Ital. Biol.* 122:83–113.

Pomeroy, S. L., A. S. LaMantia, and D. Purves. 1990. Postnatal construction of neural circuitry in the mouse olfactory bulb. *J. Neurosci.* 10:1952–1966.

Revial, M. F., A. Duchamp, A. Holley and P. MacLeod. 1978*a*. Frog olfaction: odour groups, acceptor distribution and receptor categories. *Chem. Sens.* 3:23–33.

Revial, M. F., A. Duchamp, and A. Holley. 1978*b*. Odour discrimination by frog olfactory receptors: a second study. *Chem. Sens. Flav.* 3:7–21.

Revial, M. F., G. Sicard, A. Duchamp, and A. Holley. 1982. New studies on odour discrimination in the frog's olfactory receptor cells. I. Experimental results. *Chem. Sens.* 7:175–190.

Riedel, H., and D. Schild. 1992. The dynamics of Hebbian synapses can be stabilized by a nonlinear decay term. *Neural Networks.* In press.

Schild, D. 1986. System analysis of the goldfish olfactory bulb: spatio-temporal transfer properties of the mitral cell granule cell copmlex. *Biol. Cybern.* 54:9–19.

Schild, D. 1987. Response pattern features of mitral cells in the goldfish olfactory bulb. *Brain Res.* 405:364–370.

Schild, D. 1988. Principles of odor coding and a neural network for odor discrimination. *Biophys. J.* 54:1001–1011.

Schild, D. 1989. Whole-cell currents in olfactory receptor cells of odor *Xenopus laevis. Exp. Brain Res.* 78:223–232.

Schild, D., and J. Bischofberger. 1991. Ca^{2+} modulates an unspecific cation conductance in olfactory cilia of *Xenopus laevis. Exp. Brain Res.* 84:187–194.

Scott, J. W. 1990. Extracting information from spike trains of olfactory bulb neurons. *In* Chemosensory Information Processing. D. Schild, editor. Springer, Berlin. 277–289.

Shepherd, G.M. 1972. Synaptic organization of the mammalian olfactory bulb. *Physiol. Rev.* 52:864–917.

Sicard, G. 1986. Electrophysiological recordings from olfactory receptor cells in adult mice. *Brain Res.* 397:405–408.

Sicard, G. 1990. Receptor selectivity and dimensionality of odours at the stage of the olfactory receptor cells. *In* Chemosensory Information Processing. D. Schild, editor. Springer, Berlin. 21–32.

Sicard, G., and A. Holley. 1984. Receptor cell responses to odorants: similarities and differences among odorants. *Brain Res.* 292:283–296.

van Drongelen, W., A. Holley, and K. B. Doving. 1978. Convergence in the olfactory system: quantitative aspects of odour sensitivity. *J. Theor. Biol.* 71:39–48.

Wellis, D. P., and J. S. Kauer. 1991. Patch-clamp recordings in the salamander olfactory bulb. *ACHEMS.* 13:262.